

DISCOVERY OF A CLOSE PAIR OF FAINT DWARF GALAXIES IN THE HALO OF CENTAURUS A

D. CRNOJEVIĆ¹, D. J. SAND¹, N. CALDWELL², P. GUHATHAKURTA³, B. MCLEOD², A. SETH⁴, J. SIMON⁵, J. STRADER⁶, E. TOLOBA³

Draft version September 18, 2014

ABSTRACT

As part of the Panoramic Imaging Survey of Centaurus and Sculptor (PISCeS) we report the discovery of a pair of faint dwarf galaxies (CenA-MM-Dw1 and CenA-MM-Dw2) at a projected distance of ~ 90 kpc from the nearby elliptical galaxy NGC 5128 (CenA). We measure a tip of the red giant branch distance to each dwarf, finding $D=3.63\pm 0.41$ Mpc for CenA-MM-Dw1 and $D=3.60\pm 0.41$ Mpc for CenA-MM-Dw2, both of which are consistent with the distance to NGC 5128. A qualitative analysis of the color magnitude diagrams indicates stellar populations consisting of an old, metal-poor red giant branch ($\gtrsim 12$ Gyr, $[\text{Fe}/\text{H}]\sim -1.7$ to -1.9). In addition, CenA-MM-Dw1 seems to host an intermediate-age population as indicated by its candidate asymptotic giant branch stars. The derived luminosities ($M_V = -10.9 \pm 0.3$ for CenA-MM-Dw1 and -8.4 ± 0.6 for CenA-MM-Dw2) and half-light radii ($r_h = 1.4 \pm 0.04$ kpc for CenA-MM-Dw1 and 0.36 ± 0.08 kpc for CenA-MM-Dw2) are consistent with those of Local Group dwarfs. CenA-MM-Dw1's low central surface brightness ($\mu_{V,0} = 27.3 \pm 0.1$ mag/arcsec²) places it among the faintest and most extended M31 satellites. Most intriguingly, CenA-MM-Dw1 and CenA-MM-Dw2 have a projected separation of only 3 arcmin (~ 3 kpc): we are possibly observing the first, faint satellite of a satellite in an external group of galaxies.

Subject headings: galaxies: groups: individual (CenA) — galaxies: halos — galaxies: dwarf — galaxies: photometry

1. INTRODUCTION

The relative number and astrophysical properties of dwarf galaxies represent one of the major challenges to the widely accepted Λ +Cold Dark Matter (Λ CDM) cosmological model of structure formation. For instance, the predicted number of DM haloes around a Milky Way (MW)-sized halo exceeds the observed number by at least an order of magnitude (e.g. Klypin et al. 1999; Moore et al. 1999), and their central densities at a given mass are lower than inferred from simulations (e.g. Boylan-Kolchin et al. 2011, 2012).

Understanding these challenges has largely been left to studies of the Local Group (LG; with exceptions, e.g. Nierenberg et al. 2013) where the faintest satellite galaxies can be discovered and studied in detail. However, a diversity of halo to halo substructure is expected due to varying accretion histories (Johnston et al. 2008) and inhomogeneous reionization (Busha et al. 2010); it is also possible that the LG is an outlier in its satellite properties. A systematic study of the faint satellite populations of a large number of galaxies in a variety of environments is critical before the Λ CDM picture of galaxy formation

can be confirmed.

Pioneering studies of faint satellite systems beyond the LG have begun. The M81 group of galaxies (at $D\sim 3.6$ Mpc) has been the subject of a resolved stellar population search for satellites utilizing deep ground based imaging and *Hubble Space Telescope* (HST) follow-up (Chiboucas et al. 2009, 2013), finding satellites down to $M_V = -10$ and largely confirming the faint satellite deficit with respect to Λ CDM seen in the LG. Studies of unresolved low surface brightness satellites have additionally been undertaken for more distant groups (e.g., M101, Merritt et al. 2014), where dwarf galaxy distance measurements are still necessary to produce conclusive results.

We have begun the Panoramic Imaging Survey of Centaurus and Sculptor (PISCeS) to significantly increase the sample of massive galaxy halos with a complete census of satellites down to $M_V\sim -8$ mag. PISCeS is focused on two nearby massive galaxies – the spiral NGC253 and the elliptical NGC5128/CentaurusA (CenA), that reside in a loose group of galaxies (Sculptor) and in a rich group (CenA), respectively (see Sand et al. 2014, for more details). PISCeS will identify faint satellites and streams from resolved stellar light out to $R\sim 150$ kpc in each system, allowing for direct comparison with the MW, the M31 Pan-Andromeda Archaeological Survey (PAndAS; McConnachie et al. 2009) and M81 (Chiboucas et al. 2013). Out of the planned survey area of ~ 17 deg², we have already collected data over ~ 12 deg² around CenA.

In this *Letter*, we present the first results of our survey around CenA: the discovery of a close pair of faint dwarf galaxies, likely associated with CenA. The dwarfs were immediately visible in our PISCeS survey data and are

* This paper includes data gathered with the 6.5 meter Magellan Telescopes located at Las Campanas Observatory, Chile.

¹ Texas Tech University, Physics Department, Box 41051, Lubbock, TX 79409-1051, USA

² Harvard-Smithsonian Center for Astrophysics, Cambridge, MA 02138, USA

³ UCO/Lick Observatory, University of California, Santa Cruz, 1156 High Street, Santa Cruz, CA 95064, USA

⁴ Department of Physics and Astronomy, University of Utah, Salt Lake City, UT 84112, USA

⁵ Observatories of the Carnegie Institution for Science, 813 Santa Barbara Street, Pasadena, CA 91101, USA

⁶ Michigan State University, Department of Physics and Astronomy, East Lansing, MI 48824, USA

located near CenA’s major axis in the north-east direction, at a projected distance of 92 kpc. For the more luminous dwarf, a modest surface brightness enhancement can be recognized in archival Digital Sky Survey images.

In §2 we describe our data and reduction procedure, while in §3 we present the physical properties derived for the newly discovered dwarfs. In §4 we discuss the possibility of these dwarfs constituting a pair of galaxies and draw our conclusions.

2. OBSERVATIONS AND DATA REDUCTION

The data presented here were acquired on 2013 June 4 (UT), as part of the PISCeS survey, with Megacam (McLeod et al. 2006) at the Magellan Clay 6.5m telescope, which has a $\sim 24' \times 24'$ field of view and a binned pixel scale of $0''.16$. The seeing was excellent throughout the night, with a median of $\sim 0.55 - 0.6''$, and the conditions were photometric. The final stacked images had a total exposure time of 5×300 sec for the r -band and 6×300 sec for the g -band. Initial data reduction (image detrending, astrometry and stacking) was performed by the Smithsonian Astrophysical Observatory Telescope Data Center, using a code developed by M. Conroy, J. Roll and B. McLeod.

We perform point spread function (PSF)-fitting photometry on the final stacked images, adopting the suite of programs DAOPHOT and ALLFRAME (Stetson 1987, 1994). We construct a PSF for each band selecting ~ 450 bright stars across the image. We then fit the PSF to all objects 3σ above the background for each image, and compute the coordinate transformations between filters with DAOMATCH/DAOMASTER (Stetson 1993). Finally, we perform simultaneous photometry of all the objects detected in both filters in order to obtain deeper catalogues. We only keep those objects satisfying the criteria $|sharp| < 3$ and $\chi < 1.5$. The same night, several equatorial Sloan Digital Sky Survey fields were observed at different airmasses to obtain zeropoints, color terms and extinction coefficients, and thus calibrate the instrumental magnitudes to the SDSS system. Stars have been individually corrected for Galactic extinction (Schlafly & Finkbeiner 2011), which has an average value of $E(B - V) \sim 0.15$.

The photometric errors and incompleteness of our data have been computed via artificial star experiments. We have injected $\sim 10^6$ fake stars with a uniform distribution on each of the stacked images, divided into 20 experiments in order not to increase the stellar crowding artificially. The fake stars cover the whole relevant range in color-magnitude space, and additionally reach $r \sim 29$ mag (~ 2 mag fainter than the faintest real recovered stars). The same PSF-fitting photometry procedure used for the real data has been performed on the fake stars. We find the overall (color-averaged) 50% completeness limit to be $r \sim 25.75$ and $g \sim 26.75$. Note that in the central ~ 1 arcmin of CenA-MM-Dw1 the crowding is higher than in the rest of the pointing, and the 50% completeness limits correspond to $r \sim 25.5$ and $g \sim 26.5$.

Figure 1 shows the dereddened color magnitude diagrams (CMDs) for our newly found dwarfs, CenA-MM-Dw1 and CenA-MM-Dw2. The error bars (from the artificial star experiments) show the typical magnitude and color uncertainty as a function of r -band magnitude, and

the 50% completeness limits (for uncrowded regions) are drawn.

3. PROPERTIES OF CENA-MM-DW1 AND CENA-MM-DW2

We begin this section by broadly discussing the stellar populations of our newly found dwarfs, and visualizing these new systems via red giant branch (RGB) stellar maps. We then discuss the distance, structure, metallicity and luminosity of this faint pair of CenA dwarfs.

3.1. Stellar Populations and Red Giant Branch Map

Figure 1 shows our dereddened CMDs where stars within the half light radius (calculated in § 3.3) are plotted. The field CMDs (rescaled to the area of each dwarf) in the right panels are from 3 rectangular regions with an area of $\sim 0.1 \times 0.1$ deg² each, two of which are located ~ 10 arcmin closer/further away than our targets along CenA’s major axis (see Figure 2), and the third one located perpendicular to it, to the east of the two dwarfs. This choice is driven by the necessity of taking into account a possible density gradient and small-scale substructures in CenA’s halo. The field CMDs show the main contaminants, i.e. Galactic foreground (almost vertical) sequences at $(g - r)_0 \sim 0.5$ and ~ 1.3 , unresolved background galaxies centered at $(g - r)_0 \sim 0$, and CenA RGB halo stars (sparsely populated at these large projected galactocentric distances, ~ 90 -95 kpc).

A prominent RGB is evident for both dwarfs. We plot the overall distribution of RGB stars in the Megacam field in Figure 2, utilizing all stars from the red selection box in the CMDs (Figure 1). These predominantly old stars are clearly clumped at the position of the dwarfs (Figure 2, right panel). We cannot rule out the presence of younger, main sequence stars: for CenA-MM-Dw2, a $\sim 1\sigma$ excess of blue sources can be seen at the center of the dwarf, but we do not consider this conclusive due to the strong background galaxy contamination. CenA-MM-Dw1’s CMD shows an overdensity of sources above the RGB with respect to foreground contaminants, which may be luminous asymptotic giant branch stars. If real, they belong to an episode of star formation that occurred $\sim 1 - 8$ Gyr ago. A more definitive assessment of the dwarfs’ star formation history will be forthcoming after planned HST observations of the pair.

3.2. Distances to the new dwarfs

We derive the distance to the new dwarfs using the tip of the RGB (TRGB) method, which utilizes the brightest, metal poor RGB stars as a standard candle (e.g. Lee et al. 1993; Salaris et al. 2002; Rizzi et al. 2007). We employ a Sobel edge detection filter to identify a sharp transition in the r -band luminosity function, with a color cut of $0.8 < (g - r)_0 < 1.2$ in order to minimize contamination from foreground Galactic stars (at red colors) and unresolved background galaxies (bluer than the RGB).

We find $r_{0,TRGB} = 24.79 \pm 0.22$ for CenA-MM-Dw1 and $r_{0,TRGB} = 24.77 \pm 0.22$ for CenA-MM-Dw2, where the errors mainly depend on photometric uncertainties rather than the number of stars. These values correspond to distance moduli of $(m - M)_0 = 27.80 \pm 0.24$ and $(m - M)_0 = 27.78 \pm 0.24$, respectively, once adopting a theoretically calibrated TRGB absolute value of $M_r^{TRGB} = -3.01 \pm 0.1$ (as computed in Sand et al. 2014

for SDSS bands). As a test, we derive TRGB distances for the adopted field regions, i.e. for stars belonging to CenA’s outer halo. We obtain $(m-M)_0 = 27.85 \pm 0.28$, in excellent agreement with the average of literature values using several methodologies $((m-M)_0 = 27.91 \pm 0.05$; Harris et al. 2010). The derived distances put the two dwarfs at roughly the same distance as CenA, thus suggesting they are its satellites. Follow-up HST data will be used to refine these distances and investigate the possibility that the two dwarfs form a physical pair (see discussion in § 4).

3.3. Structural parameters and luminosities

To quantify the structure and luminosities of our new dwarf discoveries, we work with RGB stars from the selection boxes shown in Figure 1. First, the dwarf centers are determined via an iterative process, computing the average of the stellar positions within circles of decreasing radius. From there, the position angle and ellipticity are measured using the method of moments for the RGB spatial distributions (e.g. McLaughlin et al. 1994). The final values are reported in Table 1. For CenA-MM-Dw2 we only obtain upper limits on the ellipticity (and thus have a poorly determined position angle) because of the low number of available stars.

We derive radial density profiles by counting the number of RGB stars in elliptical (circular) radii for CenA-MM-Dw1 (CenA-MM-Dw2). The field level is estimated from the average number of RGB stars present in our adopted field regions, and is entirely consistent with the number density for CenA-MM-Dw1 beyond ~ 4.5 arcmin. We subtract the field level from the derived radial profiles and correct them for incompleteness (including a correction for the excess crowding incompleteness within ~ 1 arcmin of CenA-MM-Dw1).

Given the faint nature of these dwarfs, resolved RGB stars are necessary to trace their radial profiles as opposed to integrated light. However, we adopt the latter to convert the observed number density into proper surface brightness values. This can be done by performing integrated aperture photometry in the central regions of the dwarfs, and scaling the number density profile to the central surface brightness values (e.g., Barker et al. 2009; Bernard et al. 2012; Crnojević et al. 2014). The zero-point between the two profiles is computed from their overlapping region, i.e. the innermost $\sim 0.2/0.1$ arcmin for CenA-MM-Dw1 and CenA-MM-Dw2, respectively. The integrated light photometry is performed by summing up the flux within these apertures, subtracting the median sky level and applying zeropoint, color terms and airmass corrections (Sect. 2). The composite surface brightness profiles are shown in Figure 3. Note that we reach a remarkable surface brightness of $\mu_r \sim 31$ mag/arcsec² (before field subtraction).

Sérsic models are fit via least squares minimization to the composite surface brightness profiles (Figure 3), for datapoints within ~ 3 arcmin for CenA-MM-Dw1 and ~ 0.5 arcmin for CenA-MM-Dw2. Beyond these radii, the profile of each dwarf is contaminated by the light of the other dwarf (CenA-MM-Dw2 can be recognized as an enhancement in CenA-MM-Dw1’s profile at ~ 4 arcmin). The resulting parameters of the Sérsic profiles are reported in Table 1, and are consistent with being exponential profiles.

The uncontaminated profiles trace out to ~ 2 times the derived half-light radii for the dwarfs. We derive their luminosities by integrating the best-fit Sérsic profiles, and obtain $M_r = -11.2 \pm 0.3$ for CenA-MM-Dw1 and $M_r = -8.9 \pm 0.6$ for CenA-MM-Dw2 (uncertainties from error propagation). Using the transformation between SDSS and Johnson-Cousins filters reported by Jester et al. (2005), the V -band total magnitudes of the dwarfs are $M_V = -10.9 \pm 0.3$ for CenA-MM-Dw1 and -8.4 ± 0.6 for CenA-MM-Dw2.

3.4. Metallicities

The two dwarfs host relatively metal-poor stellar populations, as can be seen from the isochrones overplotted on the CMDs in Figure 1. To quantify this, we use the standard method for computing photometric metallicities (e.g. Crnojević et al. 2010): we interpolate between solar-scaled isochrones with a fixed age of 12 Gyr and $[\text{Fe}/\text{H}]$ varying from -2.5 to -1.1 , adopting the Dartmouth stellar evolutionary database (Dotter et al. 2008). A metallicity value is obtained for each individual RGB star with magnitude $r_0 < 25.5$. The mean values we deduce are $[\text{Fe}/\text{H}] \sim -1.7$ for CenA-MM-Dw1 and $[\text{Fe}/\text{H}] \sim -1.9$ for CenA-MM-Dw2 (as plotted in Figure 1). The spread of the RGB is consistent with photometric errors, however we cannot exclude an intrinsic range of metallicities for CenA-MM-Dw1 in particular. Follow-up data will be crucial to assess the metallicity content of these dwarfs more precisely.

4. DISCUSSION AND CONCLUSIONS

We have presented the discovery of a faint pair of (likely) satellites of the elliptical galaxy CenA, discovered within our PISCeS survey. CenA-MM-Dw1 and CenA-MM-Dw2 are located at a projected distance of 92 kpc from the center of their parent galaxy and lie at its approximate distance ($\sim 3.6 \pm 0.4$ Mpc), although the uncertainties call for deeper photometric follow-up. Both dwarfs contain predominantly old (~ 12 Gyr) and metal-poor stellar populations ($[\text{Fe}/\text{H}] \sim -1.9/-1.7$), while CenA-MM-Dw1 likely also contains intermediate age asymptotic giant branch stars. Neither CenA-MM-Dw1 or CenA-MM-Dw2 are detected in the HI Parkes All Sky Survey (HIPASS; Barnes et al. 2001), with 3σ upper mass limits of $M_{\text{HI}} \lesssim 4 \times 10^7 M_\odot$.

The derived structural and luminosity parameters of CenA-MM-Dw1 and CenA-MM-Dw2 (Table 1) place them within the main locus defined by MW and M31 dwarfs with similar properties (Figure 4). Of some note is the low central surface brightness of CenA-MM-Dw1 ($\mu_{V,0} = 27.3$ mag/arcsec²), which lies at the edge of the M31 satellites distribution in a surface brightness versus luminosity plot. Its properties are comparable to a few M31 satellites (AndXXIII, AndXIX, LacI and CasIII; McConnachie 2012; Martin et al. 2013) with large half light radii ($\gtrsim 1$ kpc) and unusually low central surface brightness ($\mu_{V,0} \gtrsim 26 - 28$ mag/arcsec²). No MW satellite shows such a low central surface brightness and large half light radius at the same time. It has been suggested that M31 companions with $M_V > -9$ have lower surface brightness and are more extended with respect to MW companions with similar luminosity (Kalirai et al. 2010), although the inclusion of the latest results for the

M31 subgroup have substantially decreased this difference (Tollerud et al. 2012).

The new dwarfs’ distances are consistent with each other, and their very small angular separation (3 arcmin or 3.1 kpc at the distance of the dwarfs) suggests we are looking at the first, faint satellite of a satellite in an external group of galaxies. According to simulations, groups of dwarfs infalling into the potential well of a giant host are common (D’Onghia & Lake 2008), although the predicted pairs of satellites (with comparable luminosities) are fewer than those observed in the LG (e.g. Fattahi et al. 2013).

Examples of dwarf associations are present within the LG: the Magellanic Clouds, NGC147/NGC185 (Fattahi et al. 2013; Crnojević et al. 2014, but see also Watkins et al. 2013), Leo IV/Leo V/Crater (Belokurov et al. 2008; de Jong et al. 2010; Belokurov et al. 2014, but see Sand et al. 2010, 2012; Jin et al. 2012), and for all these pairs a common infall to the LG has been suggested (Evslin 2014). Note that all the galaxies within these pairs display similar luminosities, while CenA-MM-Dw1 is ~ 2.5 mag brighter than CenA-MM-Dw2. In some cases, stellar streams/overdensities with small angular separation are interpreted as dynamically associated structures, or even remnants of infalling groups onto the MW’s halo, where the most massive of the dwarfs has already been disrupted (Belokurov et al. 2009; Deason et al. 2014, and references therein). Deason et al. (2014) suggest that 30% of faint dwarfs are likely to have fallen onto the MW as satellites of more massive dwarfs.

For some of the cited pairs, tidal perturbances/streams have been observed, even though their origin is still un-

der discussion. Intriguingly, CenA-MM-Dw2 lies only ~ 3 arcmin in projection away from its more massive companion and does not display clear signs of distortion, however the upper limit for its ellipticity ($\epsilon = 0.67$) is high, and possible substructures may be hiding at fainter magnitudes. We compute CenA-MM-Dw1’s tidal radius from a King profile, obtaining 6.3 ± 0.9 kpc, while its Jacobi radius is $2.2 \pm 0.3 - 4.7 \pm 0.5$ kpc (assuming $(M/L)_V = 10 - 100$, a projected radius from CenA of 92 kpc and a CenA mass of $0.5 \times 10^{12} M_\odot$, Karachentsev et al. 2007), thus CenA-MM-Dw2 may be within its gravitational influence. The CMDs derived from deeper HST imaging will allow for an improved rejection of background galaxies, and thus a more accurate investigation of CenA-MM-Dw2’s structural parameters and possible tidal distortions. If this speculation is confirmed, we might be looking at the last moments of CenA-MM-Dw2 before it is accreted by its more massive companion CenA-MM-Dw1.

ACKNOWLEDGEMENTS

We warmly thank Maureen Conroy, John Roll and Sean Moran for their prolonged efforts and help related to Megacam. DC wishes to kindly thank the hospitality of the Mullard Space Science Laboratory, University College of London, where part of this work has been carried out. DJS, JS and PG acknowledge support from NSF grant AST-1412504; PG acknowledges additional support from NSF grant AST-1010039. This paper uses data products produced by the OIR Telescope Data Center, supported by the Smithsonian Astrophysical Observatory.

REFERENCES

- Barker, M. K., Ferguson, A. M. N., Irwin, M., Arimoto, N., & Jablonka, P. 2009, *AJ*, 138, 1469
- Barnes, D. G., Staveley-Smith, L., de Blok, W. J. G., et al. 2001, *MNRAS*, 322, 486
- Belokurov, V., Irwin, M. J., Koposov, S. E., et al. 2014, *MNRAS*, 441, 2124
- Belokurov, V., Walker, M. G., Evans, N. W., et al. 2008, *ApJ*, 686, L83
- . 2009, *MNRAS*, 397, 1748
- Bernard, E. J., Ferguson, A. M. N., Barker, M. K., et al. 2012, *MNRAS*, 426, 3490
- Boylan-Kolchin, M., Bullock, J. S., & Kaplinghat, M. 2011, *MNRAS*, 415, L40
- . 2012, *MNRAS*, 422, 1203
- Busha, M. T., Alvarez, M. A., Wechsler, R. H., Abel, T., & Strigari, L. E. 2010, *ApJ*, 710, 408
- Chiboucas, K., Jacobs, B. A., Tully, R. B., & Karachentsev, I. D. 2013, *AJ*, 146, 126
- Chiboucas, K., Karachentsev, I. D., & Tully, R. B. 2009, *AJ*, 137, 3009
- Crnojević, D., Ferguson, A. M. N., Irwin, M. J., et al. 2014, *MNRAS*, submitted
- Crnojević, D., Grebel, E. K., & Koch, A. 2010, *A&A*, 516, A85
- de Jong, J. T. A., Yanny, B., Rix, H., et al. 2010, *ApJ*, 714, 663
- Deason, A. J., Belokurov, V., Hamren, K. M., et al. 2014, *ArXiv e-prints*, arXiv:1407.4458
- D’Onghia, E., & Lake, G. 2008, *ApJ*, 686, L61
- Dotter, A., Chaboyer, B., Jevremović, D., et al. 2008, *ApJS*, 178, 89
- Evslin, J. 2014, *MNRAS*, 440, 1225
- Fattahi, A., Navarro, J. F., Starkenburg, E., Barber, C. R., & McConnachie, A. W. 2013, *MNRAS*, 431, L73
- Harris, G. L. H., Rejkuba, M., & Harris, W. E. 2010, *PASA*, 27, 457
- Jester, S., Schneider, D. P., Richards, G. T., et al. 2005, *AJ*, 130, 873
- Jin, S., Martin, N., de Jong, J., et al. 2012, in *Astronomical Society of the Pacific Conference Series*, Vol. 458, *Galactic Archaeology: Near-Field Cosmology and the Formation of the Milky Way*, ed. W. Aoki, M. Ishigaki, T. Suda, T. Tsujimoto, & N. Arimoto, 153
- Johnston, K. V., Bullock, J. S., Sharma, S., et al. 2008, *ApJ*, 689, 936
- Kalirai, J. S., Beaton, R. L., Geha, M. C., et al. 2010, *ApJ*, 711, 671
- Karachentsev, I. D., Tully, R. B., Dolphin, A., et al. 2007, *AJ*, 133, 504
- Klypin, A., Kravtsov, A. V., Valenzuela, O., & Prada, F. 1999, *ApJ*, 522, 82
- Lee, M. G., Freedman, W. L., & Madore, B. F. 1993, *ApJ*, 417, 553
- Martin, N. F., Slater, C. T., Schlafly, E. F., et al. 2013, *ApJ*, 772, 15
- McConnachie, A. W. 2012, *AJ*, 144, 4
- McConnachie, A. W., Irwin, M. J., Ibata, R. A., et al. 2009, *Nature*, 461, 66
- McLaughlin, D. E., Harris, W. E., & Hanes, D. A. 1994, *ApJ*, 422, 486
- McLeod, B., Geary, J., Ordway, M., et al. 2006, in *Scientific Detectors for Astronomy 2005*, ed. J. E. Beletic, J. W. Beletic, & P. Amico, 337
- Merritt, A., van Dokkum, P., & Abraham, R. 2014, *ApJ*, 787, L37
- Moore, B., Ghigna, S., Governato, F., et al. 1999, *ApJ*, 524, L19
- Nierenberg, A. M., Treu, T., Menci, N., Lu, Y., & Wang, W. 2013, *ApJ*, 772, 146
- Rizzi, L., Tully, R. B., Makarov, D., et al. 2007, *ApJ*, 661, 815
- Salaris, M., Cassisi, S., & Weiss, A. 2002, *PASP*, 114, 375
- Sand, D. J., Seth, A., Olszewski, E. W., et al. 2010, *ApJ*, 718, 530

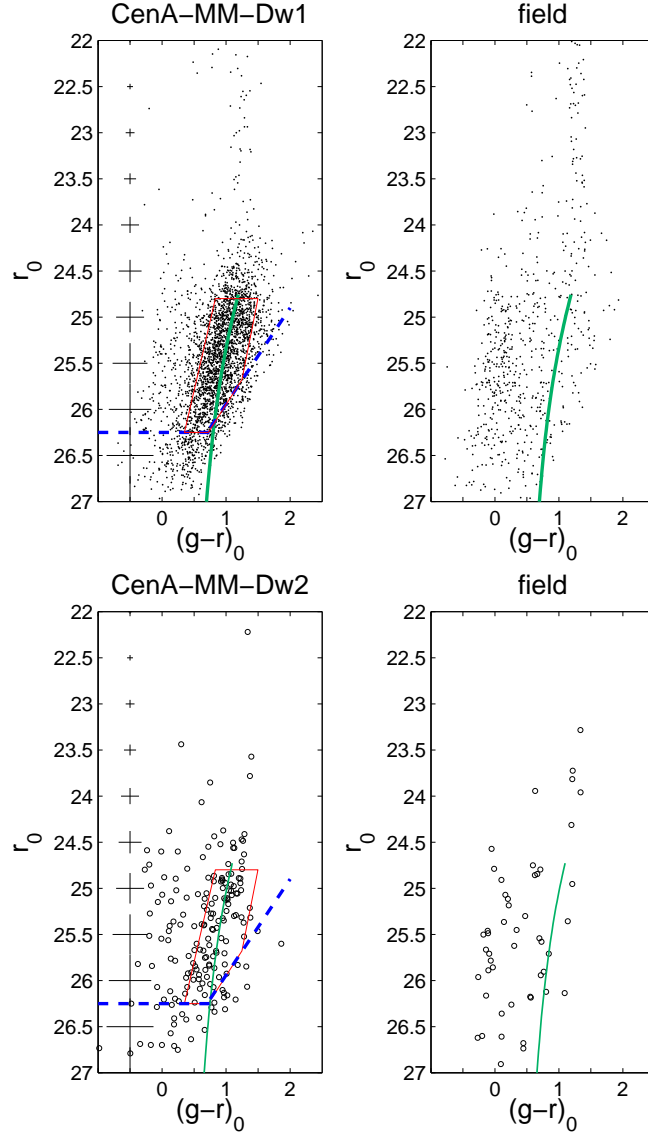


FIG. 1.— De-reddened CMDs of the two newly discovered dwarf satellites (*left panels*). Stars within the half light radius are plotted. A background field CMD with the same area as the one selected for each dwarf is shown for comparison (*right panels*). Overplotted on the clearly visible RGB for each dwarf is a Dartmouth isochrone shifted to the dwarf’s measured distance (§ 3.2), with an age of 12 Gyr and metallicity $[\text{Fe}/\text{H}] = -1.7$ for CenA-MM-Dw1 and -2.0 for CenA-MM-Dw2. The RGB selection box, utilized in Figure 2, is drawn in red. The dashed lines indicate the 50% completeness level while photometric errors stemming from artificial star tests are shown on the left side of each CMD.

Sand, D. J., Strader, J., Willman, B., et al. 2012, *ApJ*, 756, 79
 Sand, D. J., Crnojević, D., Strader, J., et al. 2014, *ArXiv e-prints*, arXiv:1406.6687
 Schlafly, E. F., & Finkbeiner, D. P. 2011, *ApJ*, 737, 103
 Stetson, P. B. 1987, *PASP*, 99, 191
 Stetson, P. B. 1993, in *IAU Colloq. 136: Stellar Photometry - Current Techniques and Future Developments*, ed. C. J. Butler & I. Elliott, 291

—. 1994, *PASP*, 106, 250
 Tollerud, E. J., Beaton, R. L., Geha, M. C., et al. 2012, *ApJ*, 752, 45
 Watkins, L. L., Evans, N. W., & van de Ven, G. 2013, *MNRAS*, 430, 971

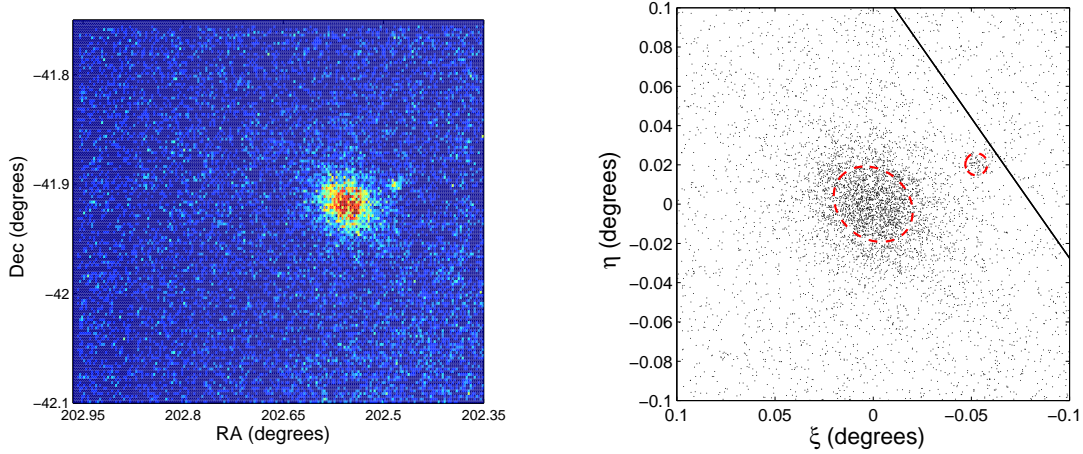


FIG. 2.— *Left panel.* Density map of all RGB stars in the considered Magellan/Megacam pointing, including all stars drawn from the selection box illustrated in Figure 1. The two newly discovered dwarf satellites are clearly visible as overdensities, only ~ 0.05 deg (~ 3 kpc) apart in projection. *Right panel.* A zoomed-in view of the spatial distribution of RGB stars centered on CenA-MM-Dw1. For CenA-MM-Dw1 (CenA-MM-Dw2) we draw a red ellipse (circle) at the half light radius and with the PA and ϵ reported in Table 1. The black line indicates the projection of CenA's major axis.

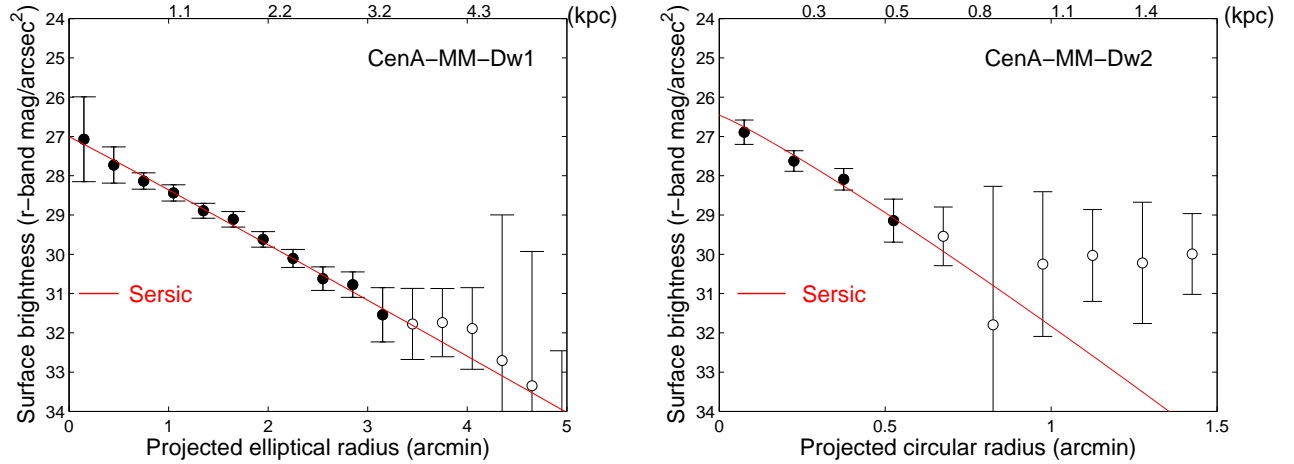


FIG. 3.— Surface brightness profiles in r -band for the two dwarfs as a function of elliptical (circular) radius for CenA-MM-Dw1 (CenA-MM-Dw2). First, the number density profiles for RGB stars have been corrected for incompleteness, and the field level has been subtracted from the profiles. Subsequently, these have been converted into surface brightness by tagging them onto the integrated photometry within the innermost $\sim 0.2/0.1$ arcmin for CenA-MM-Dw1 and CenA-MM-Dw2, respectively. Error bars are Poissonian. CenA-MM-Dw2 can be recognized in CenA-MM-Dw1's profile as an overdensity at ~ 4 arcmin, while CenA-MM-Dw1 starts to dominate CenA-MM-Dw2's profile beyond ~ 0.75 arcmin. Filled symbols indicate the datapoints included in the Sersic fit, and the best-fitting Sersic profiles are overplotted, being consistent with exponential profiles (see Tab. 1). The upper x -axes report galactocentric distances in physical units.

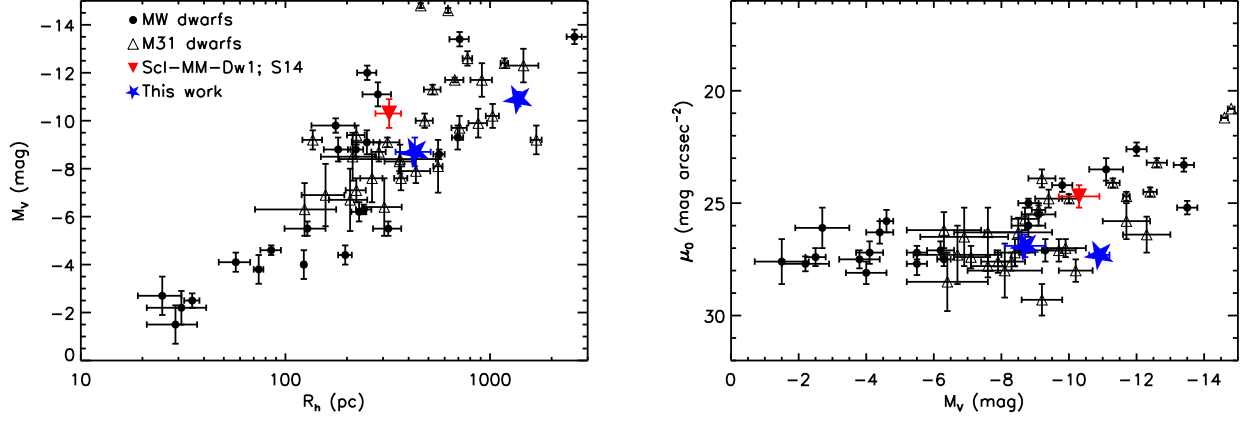


FIG. 4.— *Left panel*: Absolute V -band magnitude as a function of half-light radius for MW/M31 dwarf galaxies (black points/triangles, from McConnachie (2012) or Sand et al. (2012)), CenA-MM-Dw1 and CenA-MM-Dw2 (blue stars), and Scl-MM-Dw1 (red inverted triangle, Sand et al. 2014). *Right panel*: Central V -band surface brightness as a function of absolute magnitude. CenA-MM-Dw1's properties place it among M31 companions with the lowest central surface brightnesses and largest half-light radii.

TABLE 1
PROPERTIES OF THE NEWLY DISCOVERED DWARFS.

Parameter	CenA-MM-Dw1	CenA-MM-Dw2
RA (h:m:s)	13:30:14.26 \pm 2"	13:29:57.34 \pm 2"
Dec (d:m:s)	-41:53:35.8 \pm 10"	-41:52:22.6 \pm 10"
$(m - M)_0$ (mag)	27.80 \pm 0.24	27.78 \pm 0.24
D (Mpc)	3.63 \pm 0.41	3.60 \pm 0.41
ϵ	0.19 \pm 0.01	<0.67 ^a
PA (N to E; $^\circ$)	51.3 \pm 1.1	Unconstrained ^a
$\mu_{r,h}$ (mag/arcsec 2)	28.8 \pm 0.1	28.1 \pm 0.5
r_h (arcmin)	1.30 \pm 0.04	0.34 \pm 0.08
r_h (kpc)	1.4 \pm 0.04	0.36 \pm 0.08
n (Sersic index)	0.98 \pm 0.10	0.90 \pm 0.44
$\mu_{V,0}$ (mag/arcsec 2)	27.3 \pm 0.1	26.5 \pm 0.5
M_V (mag)	-10.9 \pm 0.3	-8.4 \pm 0.6
L_* ($10^6 L_\odot$)	2 \pm 0.5	0.2 \pm 0.1

^a Only upper limits on the ellipticity, ϵ , of CenA-MM-Dw2 were measurable, thus leaving the PA unconstrained.